Dark Energy from the Thermal Sunyaev Zeldovich Power Spectrum

Boris Bolliet,[1,2,3] Barbara Comis,[2] Eiichiro Komatsu,[4] and Juan Macias Perez[2]

[1] *École Normale Supérieure de Lyon, 46 Allée d'Italie, Lyon 69007, France*
[2] *Laboratoire de Physique Subatomique et de Cosmologie, Université Grenoble-Alpes, CNRS/IN2P3, 53, avenue des Martyrs, 38026 Grenoble cedex, France*
[3] *Jodrell Bank Centre for Astrophysics, School of Physics and Astronomy, The University of Manchester, Manchester, M13 9PL, U.K.*
[4] *Max-Planck-Institut für Astrophysik, 85740 Garching bei München, Germany*

The work presented in this paper is dedicated to the cosmological constraints that can be obtained from the thermal Sunyaev Zeldovich (tSZ) effect angular power spectrum. The numerical computations of the tSZ power spectrum is carried out with a new module added to the Boltzmann code `CLASS` which allows for a straightforward interfacing with the Markov Chain Monte Carlo (MCMC) sampler `Montepython`. We revisit the Planck Collaboration constraints on the parameter combination $\sigma_8^8\Omega_{\rm m}^3$, and show that the trispectrum contribution to the covariance matrix can not be neglected for the measured multipoles $\ell \lesssim 1000$, in agreement with a recent analysis by Horowitz and Seljak. Unlike in the Planck analysis, the whole set of cosmological parameters are sampled in our MCMC analysis, along with the mass bias $B \equiv (1-b)^{-1}$. The amplitude of the modelled tSZ power spectrum is found to scale with the parameter combination: $F \equiv \sigma_8(\Omega_{\rm m}/B)^{3/8}h^{-1/5}$. We present the constraints on the F-parameter from the Planck 2015 Compton-y parameter power spectrum data: $F = 0.487 \pm 0.013$. Interestingly, our best-fit tSZ power spectrum extrapolated at $\ell = 3000$ matches perfectly the ACT/SPT data. To accommodate the SZ constraint on F with Planck 2015 Cosmic Microwave Background (CMB) temperature anisotropy data, we find that the mass bias has to be set to $B = 1.61 \pm 0.16$, *i.e.* $(1-b) = 0.62 \pm 0.06$. In the last part of this analysis, the dark energy equation of state is set as a free parameter, w. Although the current tSZ data does not allow for the determination of w, we find that adding a prior on the Hubble parameter $h = 0.72 \pm 0.03$, corresponding to the latest local measurements, enables a constraint on w that is competitive with the one obtained from the CMB lensing data. Our results for the wCDM cosmology are: $w = -1.13 \pm 0.14$, $\sigma_8 = 0.819 \pm 0.041$ and $\Omega_{\rm m} = 0.275 \pm 0.025$, consistent with CMB constraints.

I. INTRODUCTION

The Sunyaev Zeldovich (SZ) effect [1] is a frequency dependent distortion of the cosmic microwave background (CMB) due to the inverse Compton scattering of the CMB photons off the electrons in the intra-cluster medium (ICM). The ICM is assumed to be a diffuse plasma at hydrostatic equilibrium within the dark matter potential wells. There are two main components to the SZ effect. One that is due to the internal motion of the electrons, the so-called thermal SZ effect (tSZ), and one caused by the bulk motion of the gas when the cluster is moving with respect to the CMB rest-frame, the so-called kinetic SZ effect (kSZ). The contribution from the kSZ effect is at least one order of magnitude smaller than the tSZ effect, when we compare the angular anisotropy power spectra of the CMB temperature anisotropy associated with each component. Therefore the kSZ contribution is neglected in this work.

If we assume the electrons in the ICM gas to be non-relativistic, the frequency dependence of the tSZ effect is described by the spectral function

$$g_\nu\left(x\right) = x\coth\left(x/2\right) - 4, \quad \text{with} \quad x = \frac{h\nu}{k_{\rm B}T_{\rm CMB}}. \tag{1}$$

This means that the temperature of the CMB photons that transit across a galaxy cluster is shifted by

$$\frac{\Delta T}{T_{\rm CMB}} = g_\nu y, \tag{2}$$

where the Compton-y parameter, which sets the amplitude of the effect, contains the information relative to the thermal properties of the ICM

$$y \equiv \int {\rm d}s \frac{n_{\rm e}k_{\rm B}T_{\rm e}}{m_{\rm e}c^2}\sigma_{\rm T} = \int {\rm d}s \frac{P_{\rm e}}{m_{\rm e}c^2}\sigma_{\rm T}, \tag{3}$$

where $\sigma_{\rm T}$ is the Thomson cross-section, $n_{\rm e}$ and $P_{\rm e}$ are the electron number density and pressure, respectively, and ${\rm d}s$ is the line element along the line of sight.

The most recent measurements of the all-sky y-map were performed by the Planck Collaboration in 2015. Recall that the main products of the Planck mission are temperature maps of the CMB at angular resolutions from 33 arcmin to 5 arcmin, with nine frequency bands centered at 30, 44, 70, 100, 143, 217, 353, 545 and 857 GHz. So, based on the tSZ spectral signature (1), it is possible to extract two types of information from the Planck maps.

First, one can apply a series of algorithms [2] to identify individual clusters. The Planck collaboration reported several hundreds of resolved clusters (RC) up to redshift $z \simeq 1$ and within the mass range $10^{14} - 10^{15}{\rm M}_\odot$. The mass of a candidate cluster is not directly accessible. It is

deduced from the scaling relation between the integrated Compton-y contribution over the solid angle spanned by the cluster,

$$Y \equiv \int y d\Omega \tag{4}$$

and the *over-density mass* M_{500}, with respect to the critical density of the universe. By neglecting all contributions due to non-gravitational processes, assuming spherical collapse for the dark matter halo and hydrostatic equilibrium of the ICM, a simple model to relate the physical parameters of clusters can be built [3]. The integrated Compton parameter Y can be related to the cluster total mass M through a simple power law. The $Y-M$ relation can then be tested against data and simulations [4]. However, not only hydrostatical equilibrium may not be reached, due to non-thermal pressure in the halo [5], there may also be issues related with systematics of the X-ray observations that can affect the mass estimate. To account for these facts, a free parameter, the so-called *mass bias* B, is introduced in order to translate M_{500} into the 'true' halo mass. As we shall see, the mass bias plays a crucial role for the cosmological parameter extraction from the tSZ effect.

Second, apart from the cluster catalogue, the wide sky coverage and the multiple frequency bands of the Planck mission allows to compute the all-sky Compton parameter y-map. This is done using the Modified Internal Linear Combination Algorithm (`MILCA`) and Needlet Independent Linear Combination (`NILC`) methods for components separation [6, 7]. Then, the statistical properties of the Compton y parameter can be analyzed in harmonic space, in a way similar to the CMB temperature maps. The main observable we consider here is the tow-points correlator that yields the angular anisotropy power spectra of the y-maps in harmonic space, denoted $C_\ell^{y^2}$. Note that even low mass or not individually resolved clusters also contribute to this observable, although they can not be detected individually. Higher oder correlators have also been considered in recent works [8, 9], but we chose to not discuss them, as our main focus here is to identify the best constraints that can be set on our the cosmic evolution based on the tSZ power spectrum alone. To estimate the angular power spectrum of the y-maps it is necessary to correct for the beam convolution as well as statistical noise due to mode-coupling induced by masking foreground-contaminated sky regions. For the SZ data, this is done by exploiting the `XSPECT` method [10] that uses cross-power spectra between different y-maps.

The final power spectrum obtained with this procedure does not contain exclusively the contribution from the tSZ effect associated with galaxy clusters, $C_\ell^{\rm tSZ}$. It also contains a contribution from several foregrounds: notably, the cosmic infrared background (CIB), radio sources (RS) and infrared point sources (IR). Moreover, on small angular scales ($\ell \gtrsim 1400$) the y^2 power spectrum is dominated by correlated noise (CN). The frequency dependence of the power spectra for these foregrounds can be accurately estimated using the Full Focal Plane (`FFP6`) simulations [11] and physically motivated models [12]. Nevertheless, their normalisations remain undetermined and have to be treated as free parameters. Therefore, for the measured power spectrum $\hat{C}_\ell^{y^2}$, we assume a five components model:

$$C_\ell^{y^2} = C_\ell^{\rm tSZ} + A_{\rm CIB} C_\ell^{\rm CIB} + A_{\rm IR} C_\ell^{\rm IR} + A_{\rm RS} C_\ell^{\rm RS} + A_{\rm CN} C_\ell^{\rm CN}, \tag{5}$$

where $C_\ell^{\rm CIB}$, $C_\ell^{\rm IR}$, $C_\ell^{\rm RS}$, $C_\ell^{\rm CN}$ are the foreground contaminants, tabulated and reported in table V. (A hat refers to the measured signal and no hat refer to the model.)

Since correlated noise largely dominates over other foregrounds and the tSZ component at high multipoles, its amplitude can be set by fitting the signal at $\ell = 2742$:

$$A_{\rm CN} = \hat{C}_{2742}^{y^2} / C_{2742}^{\rm CN} = 0.903, \tag{6}$$

as can be computed with the numerical values in the last line of table (V). This leaves three undetermined foreground parameters, namely $A_{\rm CIB}$, $A_{\rm IR}$ and $A_{\rm RS}$.

A crucial information can be extracted from the catalogue of confirmed clusters detected via the SZ effect: the power spectrum of the combined foregrounds can not be larger than the difference between the measured total power spectrum, $\hat{C}_\ell^{y^2}$, and the power spectrum associated with the projection of the SZ signal from resolved clusters on the y-map, $\hat{C}_\ell^{\rm RC}$. If we neglect systematic and statistical uncertainties, this means that the foreground amplitudes have to satisfy the following inequality:

$$A_{\rm CIB} C_\ell^{\rm CIB} + A_{\rm IR} C_\ell^{\rm IR} + A_{\rm RS} C_\ell^{\rm RS} + A_{\rm CN} C_\ell^{\rm CN} < \hat{C}_\ell^{y^2} - \hat{C}_\ell^{\rm RC}. \tag{7}$$

This condition is implemented in the maximum likelihood analysis for the determination of cosmological parameters based on the Planck 2015 SZ data, presented bellow.

The tSZ power spectrum $C_\ell^{\rm tSZ}$ is modeled analytically, following the halo model of Komatsu and Seljak [13]. It is sensitive to the cosmological parameters, in particular: the reduced Hubble constant, $h = (H_0/100)$; the amplitude of clustering, σ_8 ; the matter density parameter $\Omega_{\rm m} = 1 - \Omega_{\rm de}$; and the equation of state parameter of dark energy, $w_{\rm de}$.

In the next section, the main steps of the calculation of the tSZ power spectrum and its numerical implementation are recalled. This includes a discussion on the use of the concentration mass relations for the virial mass to overdensity mass conversion. In section III, we present the settings of our MCMC analysis and we show the importance of the non-gaussian contribution to the covariance matrix. Our results regarding cosmological constraints are given in section IV: we start by revisiting the Planck 2015 analysis, then we include the trispectrum in

the covariance matrix and finally we perform a MCMC sampling were the mass bias as well as the six cosmological parameters are varying. In the last part of section IV, we explore the constraining power of the tSZ data with respect to the equation of state parameter of dark energy. In section V, we summarise our main results and conclusions.

II. ANALYTICAL MODEL FOR THE THERMAL SUNYAEV ZELDOVICH POWER SPECTRUM

In this section we describe our model for the computation of the tSZ angular power spectrum. The main ingredients are the halo mass function (HMF), the pressure profile of the ICM and the linear matter power spectrum. We consider only the 1-halo contribution, as the 2-halo term contribution to the tSZ power spectrum is not significant, given the precision of the current data, see *e.g.* [14].

For the numerical calculations of the tSZ power spectrum (and trispectrum), we have developed a version of `class` augmented with a tSZ module. The code is dubbed `class_sz` and is available on the internet [1]. Our code agrees with the fortran code `szfast` [15] within one percent for the the computation of the tSZ power spectrum.

The tSZ angular power spectrum is calculated via an integration over mass and redshift of the two dimensional Fourier transform of the halo pressure profile,

$$C_\ell^{\rm tSZ} = \int_{z_{\rm min}}^{z_{\rm max}} {\rm d}z \frac{dV}{dz} \int_{\ln M_{\rm min}}^{\ln M_{\rm max}} d\ln M \frac{dn}{d\ln M} \left|y_\ell\left(M,z\right)\right|^2 , \tag{8}$$

where V is the comoving volume of the universe per steradian. Its derivative with respect to redshift is expressed as

$$\frac{dV}{dz} = \left(1+z\right)^2 d_{\rm A}\left(z\right)^2 cH_0/H\left(z\right). \tag{9}$$

In our code, the integration over redshift is carried out with a simple trapezoidal rule from $z_{\rm min}=0$ and up to $z_{\rm max}=6$. At higher redshift the number density of halos is vanishingly small. In fact setting $z_{\rm max}=3$ as in [16] also gives accurate results.

The integration over the mass is performed using a Gaussian quadrature method within the mass range determined by

$$M_{\rm min} = 10^{11}h^{-1}{\rm M}_\odot \quad \text{and} \quad M_{\rm max} = 5\times10^{15}h^{-1}{\rm M}_\odot. \tag{10}$$

[1] website: https://github.com/borisbolliet

The two dimensional Fourier transform of the halo pressure profile reads as

$$y_\ell = \frac{\sigma_{\rm T}}{m_{\rm e}c^2}\frac{4\pi r_{500}}{\ell_{500}^2}\int_0^{+\infty} {\rm d}x x^2 \frac{\sin\left(\ell x/\ell_{500}\right)}{\ell x/\ell_{500}} P_{\rm e}\left(x\right), \tag{11}$$

where $x\equiv r/r_{500}$ with r the radial distance to the center of the halo, r_{500} the radius of the sphere containing the overdensity mass $M_{500{\rm c}}$ with respect to the critical density of the universe, and $\ell_{500}\equiv d_{\rm A}/r_{500}$ with $d_{\rm A}\left(z\right)$ the physical angular diameter distance at redshift z. For the pressure profile, we use a standard generalized Navarro-Frenk-White (NFW) functional:

$$P_{\rm e}\left(x\right) = C\times P_0\left(c_{500}x\right)^{-\gamma}\left[1+\left(c_{500}x\right)^\alpha\right]^{(\gamma-\beta)/\alpha}, \tag{12}$$

where C is a dimension-full quantity that depends on the over-density mass $M_{500{\rm c}}$ (via the $Y-M$ scaling relation). It is given by

$$C = 1.65h_{70}^2\left(H/H_0\right)^{8/3}\left[\frac{h_{70}M_{500{\rm c}}}{3\times10^{14}{\rm M}_\odot}\right]^{2/3+0.12} {\rm eV\,cm^{-3}}. \tag{13}$$

The reader is referred to Appendix D of [17] for further details regarding this parametrization.

In our main analysis, the values of $\{\gamma,\alpha,\beta,P_0,c_{500}\}$ are set to their best-fit values obtained within the Planck 2013 (P13) analysis of clusters X-ray data [18]. In `class_sz`, the best-fit pressure profile of Arnaud *et al* 2010 (A10) [19], based on XMM Newton data set, is also readily available. The user may also specify custom values of the NFW parameters. To account for the differences in mass estimates from weak-lensing and X-rays observation, we use a mass bias B to rescale the over-density mass $M_{500{\rm c}}$ used in the Fourier transform if the pressure profile as $M_{500{\rm c}} := M_{500{\rm c}}/B$. Note that this rescaling not only affects the normalization of the pressure profile but also its scale dependence via ℓ_{500}.

Numerically, the integral in (12) is performed with Romberg's method between $x=10^{-6}$ and $x=10$. To speed up our MCMC analysis, since we were not interested in varying the NFW parameters in this work, we have tabulated the Fourier transform of the P13 and A10 pressure profiles. The python code for the interpolation, and the tabulations, can be found in the subdirectory `sz_auxiliary_files` of `class_sz`.

The differential number density of halos in Eq. (8) depends on both mass and redshift and is written as

$$\frac{dn}{d\ln M} = -\tfrac{1}{2}f\left(\sigma\right)\frac{\rho_{\rm m}\left(z_{\rm min}\right)}{M}\frac{d\ln\sigma^2}{d\ln M} \tag{14}$$

where σ^2 is the variance of the matter over-density field over a sphere of radius $R\left(M,z\right)\equiv\left[3M/4\pi\rho_{\rm m}\left(z\right)\right]^{1/3}$, *i.e.*

$$\sigma^2\left(M,z\right) \equiv \int_0^\infty \frac{dk}{k}\frac{k^3}{2\pi^2}P\left(k,z\right)W\left(kR\right)^2 \tag{15}$$

where $P(k)$ is the linear matter power spectrum, W is the top-hat window function and $f(\sigma)$ is the so-called halo mass function (HMF) whose parametrisation can be deduced from N-body simulations.

To simplify the task of accounting for the redshift dependency, $\sigma^2(M,z)$ can be factorized as

$$\sigma^2(M,z) = \sigma^2(M,z_{\rm min}) \times \left[D(z_{\rm min})/D(z)\right]^2 \qquad (16)$$

where $D(z)$ is the linear growth rate for matter perturbations.

Then, instead of $\sigma^2(M,z)$, one can introduce an auxiliary variable, $\nu(M,z)$, defined via $\nu(M,z) = \delta^2_{\rm crit}/\sigma^2(M,z)$, where $\delta_{\rm crit} = 1.6865$ is the critical over-density for spherical collapse [20]. Since the HMF, now a function of ν, is generally parametrized in terms of the over-density mass $M_{\rm X}$, we apply a chain rule:

$$\begin{aligned}\frac{dn}{d\ln M} &= \frac{d\ln M_{\rm X}}{d\ln M}\frac{dn(M_{\rm X},z)}{d\ln M_{\rm X}} \\ &\approx \frac{d\ln M_{\rm X}}{d\ln M}\frac{1}{8\pi R^3}\frac{d\ln\sigma^2}{d\ln R} f(\nu)\end{aligned} \qquad (17)$$

with $R \equiv \left[3M_{\rm X}/4\pi\rho_{\rm m}(z_{\rm min})\right]^{1/3}$, where $\nu := \nu(M_{\rm X},z)$ and where we assumed $d\ln M_{\rm X}/d\ln M \approx 1$ for the second equality [15]. In fact, to write $dn/d\ln M$ in this manner, an interpolation of $\sigma^2(M_{\rm X},z_{\rm min}) = \sigma^2(R)$ is needed for all masses $M_{\rm X}$ between $M_{\rm min}$ and $M_{\rm max}$, so one can deduce ν and subsequently evaluate the HMF. A similar interpolation for $d\ln\sigma^2/d\ln R$ is required. In our code, to obtain the interpolating functions for σ^2 and its derivative, given the linear matter power spectrum $P(k)$ computed at $z = z_{\rm min}$, we evaluate $\sigma^2(R)$ at various radii R between $R_{\rm min} = 0.0034h^{-1}$Mpc ($M_1 \simeq 1.8\times10^4 {\rm M}_\odot$) and $R_{\rm max} = 54.9h^{-1}$Mpc ($M_2 \simeq 7.5\times10^{16}{\rm M}_\odot$).

At each R within this range, the integral (15) is performed with Romberg's method. Eventually, the interpolation for σ^2 and its derivative with respect to R is obtained in terms of Chebyshev polynomials.

In `class_sz`, we have implemented four different parameterisations of the HMF: (i) the Bocquet *et al.* 2015 (B15) calibration obtained with the `Magneticum` simulations, that captures the impact of baryons [21], as our main model; (ii) the Tinker *et al.* 2008 (T08) parametrization which is based on `GADGET2` simulations [22]; (iii) the Tinker *et al.* 2010 (T10) calibration, an updated version of T08 [20] ; (iv) the Jenkins *et al.* 2001 (J01) parameterisation [23]. For instance, B15 or T08 HMF's are expressed as

$$f(\sigma) = A\left[\left(\frac{\sigma}{b}\right)^{-a}+1\right]\exp\left(-\frac{c}{\sigma^2}\right), \qquad (18)$$

with $\sigma = \delta_{\rm crit}/\sqrt{\nu}$. The phenomenological parameters entering the HMF's are redshift dependent. The redshift dependency is generally parameterized via $p = p_0(1+z)^{p_z}$ for a parameter $p = A, a, b, c$.

Like we saw in formula (17), the HMF is specified in terms of the over-density mass $M_{\rm X}$. This could be *e.g.* $M_{\rm 200m}$ (over-density with respect to the mean matter density), $M_{\rm 180m}$ as for the J01 HMF, or $M_{\rm 500c}$ (over-density with respect to the critical density). Different strategies, corresponding to different choices of $M_{\rm X}$ for the the HMF have been employed for the calculation of the tSZ power spectrum:

- The Planck Collaboration [8], as well as the authors of [9, 16], have chosen to perform the integral in (8) with the mass M being understood as $M_{\rm 500c}$. Then, no conversion is needed to compute the pressure profile which takes $M_{\rm 500c}$ as an input. The HMF chosen by the authors of the aforementioned papers is always T08. In the Tinker et al article [22] (and in the reference for the updated T10 HMF too), the parameters of the HMF are tabulated for different over-density masses. Hence, by an interpolation, it is possible to deduce the HMF parameters values corresponding to $M_{\rm 500c}$. This procedure is one of the implementations available in `class_sz`, and we refer to the code for further details on the conversion and interpolation.

- In `szfast` based articles, such as [14, 15, 21], the mass being integrated over is the virial mass $M_{\rm vir}$. A conversion from the virial mass to the over-density mass is needed twice: for the HMF and for the pressure profile. The conversion is carried out using the *Concentration-Mass* (CM) relation for dark matter halos, such as the one obtained in Duffy *et al* 2008 (D08) [24]. In `class_sz`, we have implemented several CM relations, including D08, Klypin *et al* 2010 (K10) [25], Sanchez-Conde *et al* 2014 (SC14) [26] and Zhao *et al* 2009 (Z09) [27]. Again, for further details regarding the conversion method the reader is refered to our code.

These two strategies have led to different conclusions regarding the cosmological parameter constraints obtained from the SZ power spectrum data. In particular, `szfast` based analysis have found a higher value of σ_8 than the Planck Collaboration, by about two standard deviations. Here we show that *this discrepancy is not due to the use of different HMF as claimed in [21] but, in fact, to the ambiguity of the use of the CM relation.*

On figure 1 we present the tSZ power spectrum computed in different setting. First, we observe on the top-left panel that the choice of the pressure profile is of no importance for $\ell < 10^3$. Second, on the top-right panel we see that the choice of the HMF does affect slightly the amplitude of the power spectrum. It is true that B15 yields a smaller power spectrum than T08 or T10 when the HMF are evaluated at $M_{\rm 200m}$, but this difference is

too small to explain the discrepancy on the σ_8 constraints obtained by the Planck Collaboration and `szfast` based analysis. The bottom panels correspond to the tSZ power spectrum computed using T08 HMF at the over-density mass $M_{1600\mathrm{m}}$ (left panel) and $M_{200\mathrm{m}}$ (right panel) for several CM relations. This means that the mass integration is performed over the virial mass, converted to the over-density mass $M_{200\mathrm{m}}$ or $M_{1600\mathrm{m}}$ for the HMF and to $M_{500\mathrm{c}}$ for the pressure profile, via the CM relations. When the HMF is specified at $M_{1600\mathrm{m}}$, all the results are consistent for the multipole range of interest $\ell < 10^3$. This is expected because with $\Omega_\mathrm{m} \simeq 0.3$, one has $M_{1600\mathrm{m}} \simeq M_{500\mathrm{c}}$, so that the mass that is used for the pressure profile is actually almost the same as the mass used in the HMF. But when the HMF is specified at $M_{200\mathrm{m}}$, all the results disagree. This time, the amplitude of the discrepancy is significant and shall affect the constraints on cosmological parameters. In particular, we see that the D08 CM relation leads to an underestimation of the tSZ power spectrum compared to the spectrum obtained with T08 HMF computed at $M_{500\mathrm{c}}$ (and no CM relation is used) which corresponds to the solid black line on both panels. Hence, to fit the Planck SZ data the use of D08 CM relation requires a larger tSZ amplitude (larger σ_8) compared to the method used by the Planck Collaboration.

The fact that the CM relations disagree at $M_{200\mathrm{m}}$ is certainly due to the different cosmological settings of the N-body simulations which were employed to build these relations. The `szfast` method (using virial mass to over-density mass conversion) would be consistent if one would calculate a new CM relation for each particular setting of the cosmological parameters. In principle, this could be done with the `mandc` code provided by Zhao *et al* in [27]. For our analysis, we have preferred to adopt the same strategy as the Planck Collaboration and avoid the ambiguity related to the CM relation.

We shall now investigate the influence of the cosmological parameters and the mass bias on the tSZ power spectrum. This enables us to determine the parameter combination that is best measured from the y-map data.

The effects of the cosmological parameters and the mass bias on the tSZ power spectrum are illustrated in figure 2. The optical depth at reionization, τ_reio, has no impact on the amplitude of the tSZ power spectrum (less than one percent relative variation for $0.04 \leq \tau_\mathrm{reio} \leq 0.12$) and therefore it is not shown on the figure. For the multipole range of interest ($\ell < 10^3$), the equation of state (EoS) of dark energy w (bottom left panel) and the spectral index n_s (bottom right panel) have a minor effect on the amplitude of the tSZ power spectrum. When one looks at higher multipoles, the spectral index shifts the location of the peak of the power spectrum (towards smaller angular scales for larger n_s) and the EoS changes the amplitude of the peak (increase of power for larger w). The mass bias B, the Hubble parameter h, the amplitude of clustering σ_8, and the matter density parameter Ω_m are the determining parameters for the amplitude of the tSZ power spectrum. We find that the scaling of the tSZ power spectrum is well approximated by

$$C_\ell^\mathrm{tSZ} \propto \sigma_8^{8.1}\Omega_\mathrm{m}^{3.2}B^{-3.2}h^{-1.7} \quad \text{for} \quad \ell \lesssim 10^3, \tag{19}$$

in agreement with [28] for the scaling with σ_8 and Ω_m, but now accounting for B and h. This means that the parameter combination that is best measured by experiments probing the tSZ power spectrum at multipoles $\ell \lesssim 10^3$ is

$$F \equiv \sigma_8 \left(\Omega_\mathrm{m}/B\right)^{3/8} h^{-1/5}. \tag{20}$$

This is the parameter combination that we will systematically quote. Note that similarly to [8], we opted for a replacement of the decimal numbers in Eq. (19) with the closest integers. The F-parameter differs from the parameters quoted in previous works [8, 14], *i.e.* $\sigma_8\Omega_\mathrm{m}^{3/8}$. It has the advantage of accounting for the degeneracy between the amplitude of the tSZ power spectrum and the mass bias as well as the Hubble parameter. In the most recent analysis by Salvati *et al* [16] and Hurier & Lacasa [9] the degeneracy with the mass bias was taken into account, however the exponent quoted in these works is in contradiction with ours.

III. MAXIMUM LIKELIHOOD ANALYSIS

We use the SZ information contained in the y-maps in order to set constraints on cosmological parameters. To do so, we sample the parameter space via the Monte Carlo Markov Chain (MCMC) method and extract the joint posterior probability distributions for the input parameters.

The universe is assumed to be spatially flat with an effective number of ultra-relativistic species $N_\mathrm{eff} = 3.046$. The *input* cosmological parameters that are varied are: the amplitude of the primordial power spectrum of scalar curvature perturbations A_s; the spectral index of the primordial power spectrum n_s; the optical depth at reionization τ_reio; the angular size of the sound horizon at decoupling θ_s; the reduced density parameter of baryons $\Omega_\mathrm{b}h^2$; the reduced density parameter of cold dark matter $\Omega_\mathrm{c}h^2$ and w_de. Hence, h, σ_8 and Ω_m are obtained as *derived* parameters.

In addition, the amplitude of the tSZ power spectrum strongly depends on the mass bias B, via the pressure profile of the ICM. Therefore, B is also treated as an input varying parameter in this analysis. To recap, the sampled parameter space is eleven dimensional:

$$\underbrace{A_\mathrm{s}, n_\mathrm{s}, \tau_\mathrm{reio}, \theta_s, \Omega_\mathrm{b}h^2, \Omega_\mathrm{c}h^2, w, B}_{C_\ell^\mathrm{tSZ}\text{: } slow \text{ param.}}, \underbrace{A_\mathrm{CIB}, A_\mathrm{IR}, A_\mathrm{RS}}_{C_\ell^\mathrm{FG}\text{: } fast \text{ param.}} \tag{21}$$

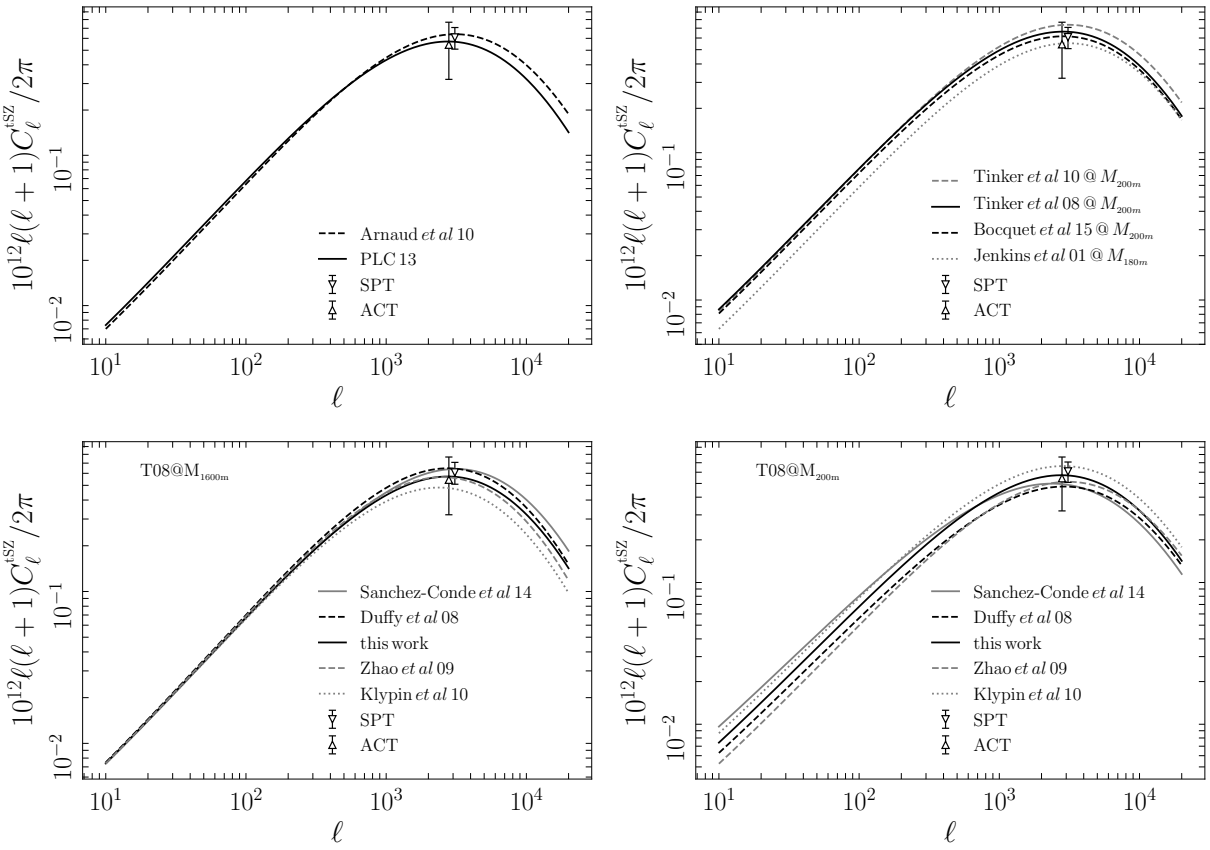

Figure 1: The tSZ power spectrum computed with `class_sz` in different settings: for two pressure profiles (top left), for several halo mass function evaluated at the over-density mass $M_{200\rm m}$ using Klypin *et al* 2010 concentration mass relation for the conversion from the virial mass to the over-density mass (top right), with the Tinker *et al* 2008 halo mass function evaluated at the over-density masses $M_{1600\rm m}$ (bottom left) and $M_{200\rm m}$ (bottom right) for several concentration mass relations. The solid black line on the bottom panels is the best-fit power spectrum to the Planck SZ data obtain from our MCMC analysis with trispectrum (the corresponding cosmological parameters best-fit values are available on the code's webpage) and computed with Tinker *et al* 2008 halo mass function evaluated at $M_{500\rm c}$, so that no concentration-mass relation is needed. The ACT and SPT data points are shown as a landmark.

with eight *slow* parameters which affect the amplitude of the tSZ power spectrum, and three *fast* parameters that set the amplitude of the foregrounds. The sampling is performed with `Montepython` [29] using the Cholesky decomposition method for an optimal treatment of fast and slow parameters [30].

Weak uniform priors are imposed on the varying parameters to avoid the sampling of unrealistic regions of the parameter space. These priors are reported in table I. For each parameter, the allowed range of value is wide enough so that changing the upper or lower bound does not affect the posterior probability distribution.

The data for the total y^2 power spectrum is deduced from the y-map of the Planck survey. It is the same as the one used for the MCMC analysis carried out by the Planck collaboration, described in [8]. We refer to this analysis as PLC15. For completeness, the Planck 2015 measured power spectrum $\hat{C}_\ell^{y^2}$ data points and error bars

	min.	max.		min.	max.		min.	max.
$10^9 A_{\rm s}$	1.8	2.7	$\Omega_b h^2$	0.0199	0.0245	$A_{\rm CIB}$	0	10
$n_{\rm s}$	0.8	1	$\Omega_c h^2$	0.09	0.15	$A_{\rm IR}$	0	10
$\tau_{\rm reio}$	0.04	0.12	w	-2	-0.5	$A_{\rm RS}$	0	10
$100\theta_s$	1.03	1.05	B	1.11	1.67			

Table I: Uniform priors imposed on the input parameter space for the MCMC analysis.

$\sigma_\ell^{y^2}$ are reported in table V. At low multipoles, the signal is contaminated by emissions from the galactic dust, while at high multipoles, the signal is dominated by correlated noise. Hence, the likelihood calculation is restricted to the effective multipole range $10 \leq \ell_{\rm eff} \leq 959.5$. The effective multipoles, $\ell_{\rm eff}$, are at the middle of the eighteen bins spanning this interval and used in PLC15. The bin sizes were chosen by minimizing the correlations be-

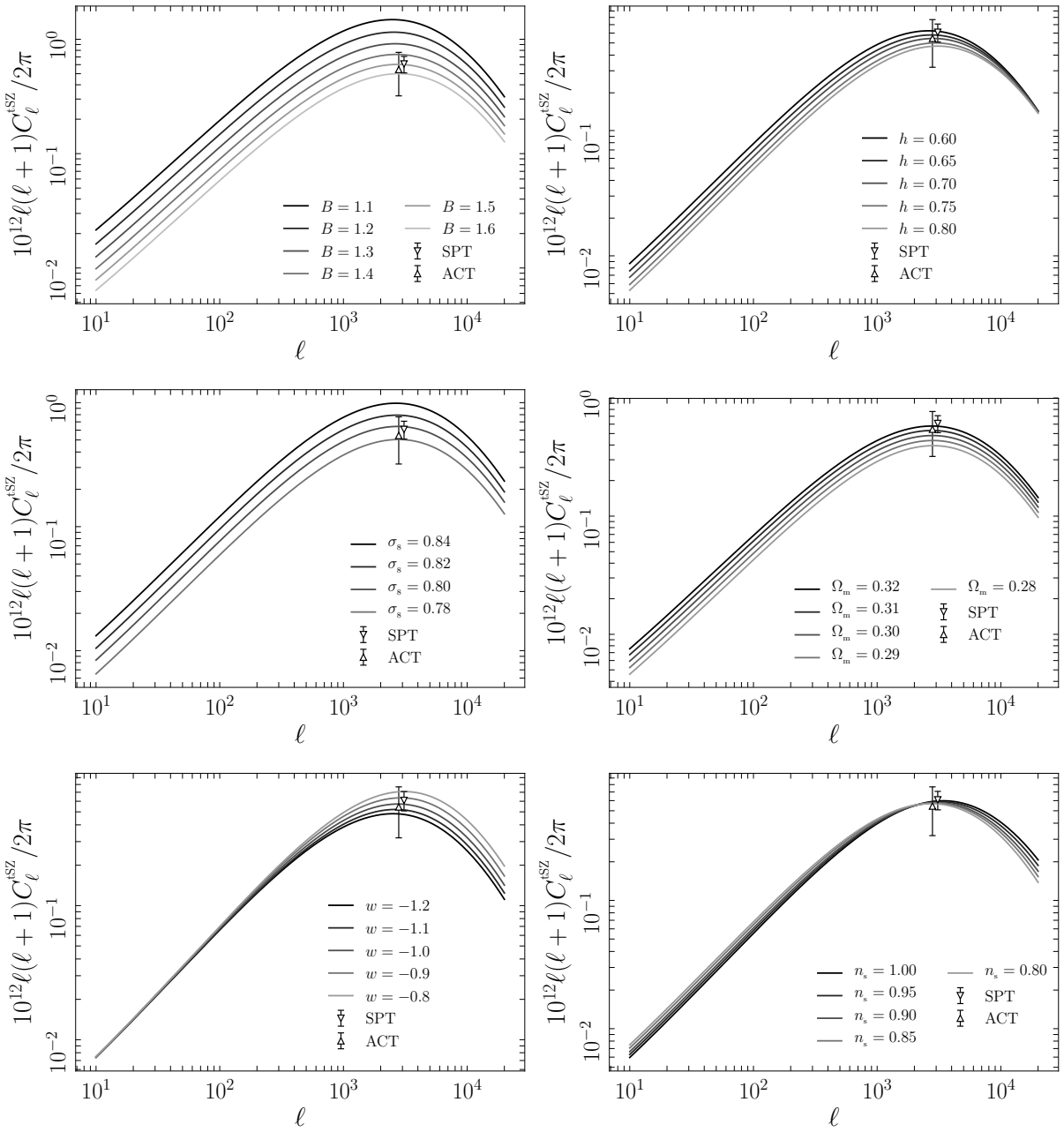

Figure 2: Influence of various parameters on the tSZ power spectrum: the mass bias B (top left); the reduced Hubble parameter h (top right); the amplitude of clustering σ_8 (middle left); the matter density parameter Ω_m (middle right); the equation of state of dark energy w (bottom left); and the spectral index n_s (bottom right). These calculations were carried out with `class_sz`. When one parameter is varied, the other are kept constant and set to their best-fit values from our MCMC analysis of the Planck 2015 SZ data (these are available on the code's webpage). The ACT and SPT data points are shown as a landmark.

tween adjacent bins at low multipole and by maximizing the signal-to-noise ratio at high multipole [28].

In addition to the uniform priors of table I, we used a rejection criterion for the amplitudes of the foreground components. Like we saw in section I, there is an upper bound for the combined foregrounds fixed by the power spectrum of the y-map obtained by projecting the confirmed clusters of the Planck 2015 SZ catalogues, $\hat{C}_\ell^{\rm RC}$ (where stands for *Resolved Clusters*). At each new proposed values for the foreground amplitudes $\{A_{\rm CIB}, A_{\rm IR}, A_{\rm RS}\}$, we ensure that the inequality in (7) is satisfied for the seven multipole bins between $\ell_{\rm eff} = 257.5$ and $\ell_{\rm eff} = 1247.5$, otherwise the point is rejected. (Above $\ell_{\rm eff} = 1247.5$ the power spectrum $\hat{C}_\ell^{\rm RC}$ is affected by the resolution of the $y-$map and can not be used. Bellow $\ell_{\rm eff} = 257.5$, statistical and systematic uncertainties are

important and (7) is no longer applicable.) The data for the power spectrum of the projected resolved clusters $\hat{C}_\ell^{\rm RC}$ and associated error bars $\sigma_\ell^{\rm RC}$ is also reported in table V, see [8, 28] for details.

At each step of the MCMC sampling, the likelihood is computed according to $-\ln\mathcal{L} = \frac{1}{2}\chi^2$ with

$$\chi^2 \equiv \sum_{a\leq a'} \left(C^{y^2}_{\ell^a_{\rm eff}} - \hat{C}^{y^2}_{\ell^a_{\rm eff}}\right) \left[M^{-1}\right]_{aa'} \left(C^{y^2}_{\ell^{a'}_{\rm eff}} - \hat{C}^{y^2}_{\ell^{a'}_{\rm eff}}\right), \tag{22}$$

where a, a' are indices for the multipole bins running from $a = 1$ ($\ell_{\rm eff} = 10$) to $a = 18$ ($\ell_{\rm eff} = 959.5$), $C^{y^2}_{\ell^a_{\rm eff}}$ is the model y^2 power spectrum, $\hat{C}^{y^2}_{\ell^a_{\rm eff}}$ are the data points and M is the binned covariance matrix.

Unlike PLC15, our covariance matrix accounts for the non-gaussian contributions, *i.e.* auto-correlations and correlations between multipole bins, arising from the tSZ *trispectrum* calculation. Hence, the coefficient of the covariance matrix relative to multipole bins a and a' reads as

$$M_{aa'} = \left(\sigma^{y^2}_{\ell^a_{\rm eff}}\right)^2 \delta_{aa'} + \frac{\ell^a_{\rm eff}\left(\ell^a_{\rm eff}+1\right)\ell^{a'}_{\rm eff}(\ell^{a'}_{\rm eff}+1)}{4\pi^2}\frac{T_{aa'}}{4\pi f_{\rm sky}}, \tag{23}$$

where $\sigma^{y^2}_{\ell^a_{\rm eff}}$ are the measured error bars (third column of table V), $f_{\rm sky} = 0.47$ is the Planck sky coverage, and $T_{aa'}$ is the binned trispectrum whose computation is detailed hereafter. The trispectrum $T_{\ell\ell'}$ of the Compton y parameter is assumed to be dominated by the tSZ effect contribution. Its computation follows the same procedure as the tSZ power spectrum, with the fourth power of the y parameter in the integrand:

$$T_{\ell\ell'} = \int {\rm d}z \frac{dV}{dz} \int {\rm d}\ln M \frac{dn}{d\ln M} \left|y_\ell\left(M,z\right)\right|^2 \left|y_{\ell'}\left(M,z\right)\right|^2, \tag{24}$$

where the redshift and mass ranges are the same as for the power spectrum, see (8). For the eighteen multipole bins of our analysis, the *binned* trispectrum that enters the covariance matrix (23) is

$$T_{aa'} = \sum_{\ell\in a}\sum_{\ell'\in a'} \frac{T_{\ell\ell'}}{N_a N_{a'}}, \tag{25}$$

where a and a' denotes two multipole bins containing respectively N_a and $N_{a'}$ multipoles.

In figure 3 we show the trispectrum against the gaussian error. As noted by Horowitz & Seljak [14], the trispectrum largely dominates the gaussian errors until $\ell \approx 500$. Moreover, as can be seen on the figure, the difference between the binned and unbinned trispectra is negligible so one can safely approximate the binned trispectrum by the unbinned value corresponding to the effective multipoles of the given bins. Hence, we can avoid the time consuming interpolation required for the binning. Both amplitudes of the power spectrum and trispectrum of the SZ effect are sensitive to the cosmological parameters h, $\Omega_{\rm m}$, σ_8 and to the mass bias B. At each step of the MCMC sampling, when a new set of parameters is proposed, the trispectrum is computed simultaneously to the power spectrum in order to deduce the likelihood (22).

The trispectrum contribution to the covariance matrix was considered in the analysis by Horowitz & Seljak [14] and Salvati *et al* [16]. However, the tSZ power spectrum data points that were used in those analysis were the one obtained in the PLC15 analysis which did not account for the trispectrum. Recall that the tSZ data points are obtained after substracting the foregrounds to the total y^2 data. Since the foreground amplitudes are estimated from the MCMC analysis, they are affected by the inclusion of the trispectrum. In the next section we present the updated tSZ data points resulting from the analysis with trispectrum. As we shall see, the trispectrum allows for larger foreground amplitudes and hence lead to a smaller tSZ amplitude lessening the tension with ACT and SPT data at $\ell = 3000$, compared to what was obtained without trispectrum in PLC15.

IV. RESULTS

In this section we present the results of three MCMC analysis. First, we performed an analysis without trispectrum in a flat ΛCDM universe. Second, we include the trispectrum in the covariance matrix. Third, we consider a wCDM cosmology and present the constraints on the equation of state parameter of dark energy obtained from the SZ data.

IV.A. Analysis without trispectrum

The Planck 2015 analysis (PLC15) did not include the trispectrum in the covariance matrix. They used T08 HMF evaluated at the over-density mass M_{500c}, along with the A10 pressure profile, allowing the foreground amplitudes as well as σ_8 and $\Omega_{\rm m}$ to vary while other parameters were set to their Planck 2013 CMB TT+lowP best-fit values. The Compton parameter was integrated between $z = 0$ and $z = 3$, the mass function between $M = 10^{13}{\rm M}_\odot$ and $M = 5\times10^{15}{\rm M}_\odot$. Two MCMC analysis without trispectrum were carried out by the Planck Collaboration. First, with a mass bias set to $B = 1.25$ ($b = 0.2$ in the notations of [8]). Second, with $B = 1.67$ (corresponding to $b = 0.4$). For $B = 1.25$, they obtained $\sigma_8\left(\Omega_{\rm m}/0.28\right)^{3/8} = 0.80^{+0.01}_{-0.03}$, while for $B = 1.67$ they get $\sigma_8\left(\Omega_{\rm m}/0.28\right)^{3/8} = 0.90^{+0.01}_{-0.03}$. The difference between the

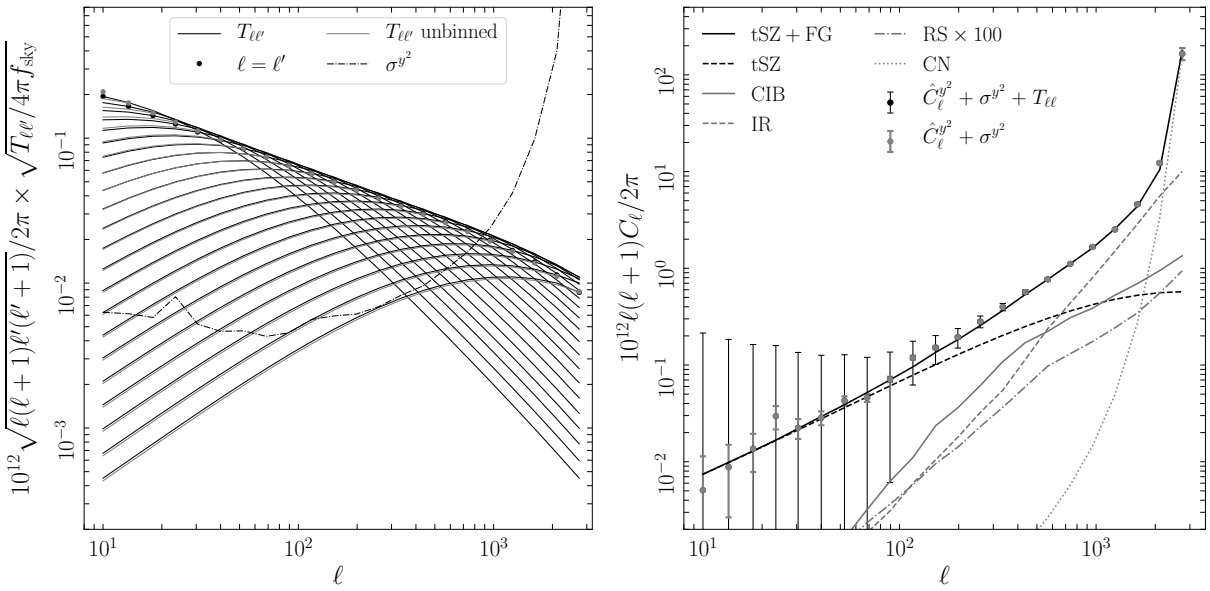

Figure 3: *Left panel:* The normalized trispectrum of the tSZ effect corresponding to the best-fit model of our MCMC analysis of the Planck 2015 SZ data (see the code's webpage for the best-fit parameter values) plotted against the gaussian error from the Planck 2015 analysis (dashed line). The binned trispectrum is shown in black and the unbinned trispectrum is shown in grey. *Right panel:* The best-fit models for the tSZ component (black dashed line) and the foregrounds (grey lines) obtained from our MCMC analysis of the Planck 2015 SZ data. The best-fit total y^2 power spectrum appears as the solid black line. The data points used in our analysis are shown in grey. The gaussian contribution to the error bars corresponds to the vertical grey lines, and the error bars that account for the trispectrum contribution, which was used in our MCMC analysis, are shown in black.

central values resulting from these two analysis is due to the degeneracy between the amplitude of the tSZ power spectrum and the mass bias, $C_\ell^{\rm tSZ} \propto B^{-3.2}$ as discussed in section II. In a preliminary analysis, we have successfully reproduced the PLC15 constraints.

For our main analysis without trispectrum, we also used T08 HMF evaluated at the over-density mass M_{500c}. We have set the pressure profile to P13 and integrated between $z = 0$ and $z = 6$, and between $M = 10^{11}h^{-1}{\rm M}_\odot$ and $M = 5 \times 10^{15}h^{-1}{\rm M}_\odot$. We allowed the six cosmological parameters to vary along with the mass bias B, and the foreground amplitudes. Since the mass bias is now taken as a varying parameter, the parameter $\sigma_8 \, (\Omega_{\rm m}/0.28)^{3/8}$ is not relevant anymore because the bounds on the marginalized posterior likelihood for this parameter are determined by the bounds on the prior distribution of the bias, namely: $B = 1.11$ and $B = 1.67$. Nevertheless, the marginalized posterior likelihood for the F-parameter defined in (20), is well approximated by a gaussian and does not depend on the choices of the input prior probability distributions. The contours are shown in red on figure 5. The F-parameter constraint is $F = 0.489 \pm 0.005$ at 68% C.L. and the foreground amplitudes are $A_{\rm CIB} = 0.44^{+0.09}_{-0.07}$, $A_{\rm IR} = 1.94^{+0.15}_{-0.14}$, $A_{\rm RS} = 0.3^{+0.06}_{-0.3}$. As we shall see in the next section, the width of the marginalized posterior probability distributions for the F-parameter and the foreground amplitudes obtained without trispectrum are largely underestimated.

IV.B. Analysis with trispectrum

When the trispectrum is included in the covariance matrix, the width of the 68% C.L. intervals is increased drastically, due to the enhanced degeneracy between the amplitude of the tSZ power spectrum with the CIB foreground at low multipoles ($\ell \lesssim 400$). The trispectrum allows for a smaller tSZ component to the y-map, corresponding to a larger CIB and IR foreground contributions to fit the signal at $\ell \gtrsim 400$, see figure 3. For the F-parameter as determined by our analysis with trispectrum we obtain

$$F = 0.487 \pm 0.013, \tag{26}$$

and the foreground amplitudes are $A_{\rm CIB} = 0.38 \pm 0.18$, $A_{\rm IR} = 2.12 \pm 0.19$, $A_{\rm RS} = 0.33^{+0.07}_{-0.33}$. The best-fit models for the tSZ and combined foregrounds are shown on figure 4 against Planck y^2 data (left panel) and ACT/SPT tSZ measurements at $\ell = 3000$ (right panel). The foreground dominate over the tSZ contribution after $\ell \approx 400$, as can be seen on the left panel. The black data points end error bars correspond to the tSZ signal obtained by marginalising over the foregrounds, and propagating the corresponding errors: $\hat{C}_\ell^{\rm tSZ} = \hat{C}_\ell^{y^2} - C_\ell^{\rm FG}$. On the

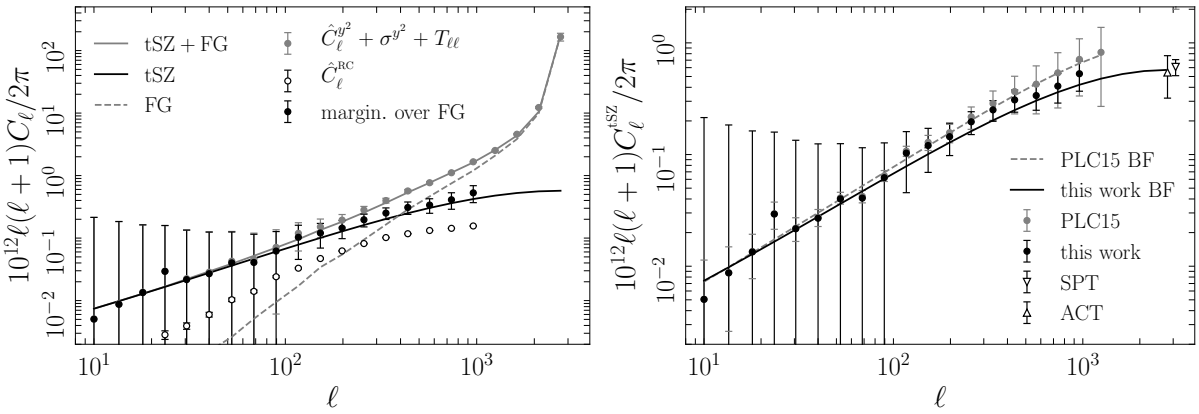

Figure 4: *Left panel:* The best-fit models for the tSZ component (solid black line) and the combined foregrounds (dashed grey line) obtained from our MCMC analysis of the Planck 2015 SZ data, extrapolated until $\ell = 3000$. The open circles correspond to projected tSZ signal from the Planck 2013 cluster catalogue. The continuous grey line is the best-fit total y^2 power spectrum. The planck 2015 data points for the y^2 power spectrum are shown in grey with the error bars that now include the trispectrum contribution. The black data points are the updated tSZ data points obtained after marginalizing the total y^2 power spectrum over the foregrounds (determined by our MCMC analysis). *Right panel:* The black data points are the updated tSZ data points obtained after marginalizing the total y^2 power spectrum over the foregrounds. The black curve is our best-fit tSZ power spectrum. The grey data points and dashed line are the results of the Planck 2015 SZ analysis. We also included the ACT and SPT tSZ data points on this plot.

right panel of the figure, we have also reported the tSZ data points obtained the PLC15 analysis with the corresponding best-fit tSZ model, against our results. Like we said, the trispectrum increases the modeled error bars at low multipoles, which leads to a lower tSZ component than without trispectrum and larger foreground amplitudes. The contours of the analysis with trispectrum are shown in black on figure 5. In addition to the broadening of the marginalized posetrior probability distributions, we see that the IR component, which dominates around $\ell = 1000$, is sensibly higher in the analysis with trispectrum. Due to this, our best-fit tSZ model flattens significantly at large multipoles compared to the best-fit model of the PLC15 analysis. Now, the best-fit tSZ model and updated data points are in an almost perfect agreement with ACT/SPT data at high multipoles. Whether this is a coincidence or an indication of the robustness of the tSZ signal modelling remains an open question, as numerical simulation continue to find a tSZ component that is about fifty percents larger than the tSZ amplitude predicted within the halo model [15].

Depending on the value of the mass bias, the tSZ constraints on the F-parameter can be conciled with CMB constraints.The Planck 2015 CMB TT+lowP chains yields $\sigma_8\Omega_{\rm m}^{3/8}h^{-1/5} = 0.582 \pm 0.016$. In fact, if we impose this constraints on $\sigma_8\Omega_{\rm m}^{3/8}h^{-1/5}$, on the F-parameter tSZ determination, we obtain an estimation of the mass bias:

$$B = 1.61 \pm 0.16, \tag{27}$$

which translate into $(1-b) = 0.62 \pm 0.06$ in the notations of *e.g.* [31, 32]. This value is in weak tension with the estimate from most numerical simulations which tend to favor $(1-b) = 0.80$. Nevertheless, it is consistent with the recent weak lensing constraint: $(1-b) = 0.73 \pm 0.10$ [32]; and in a perfect agreement with the estimate extracted in the same way from cluster number counts $(1-b) = 0.58 \pm 0.04$ [2]. We also note that for simulations where the mass dependence of the bias was investigated, it was shown that the mass bias decreases as a function of the mass towards $(1-b) \approx 0.60$ for $M \gtrsim 4 \times 10^{14} h^{-1}{\rm M}_\odot$ [33]. Our results seem to support such behavior of the mass bias, since the tSZ signal bellow $\ell \approx 10^3$ is mainly due to the most massive halos, as can be seen on figure 6.

IV.C. Constraints on Dark Energy

In this section, we present a new way of constraining the equation of state (EoS) for dark energy, w, based on the SZ cosmological data (all sky y-map) and an independent determination of the Hubble parameter. Like we saw on figure 2, the EoS does not affect the amplitude of the tSZ power spectrum in the multipole range of interest to us. Nevertheless, the tSZ power spectrum is an indirect probe of the linear matter power spectrum and therefore it implicitly probes the known degeneracy between the EoS, the Hubble parameter and the reduced matter density. Using the local measurement of the Hubble parameter deduced from up-to-date time-delay cosmography measurements of quasars, $h = 0.72 \pm 0.03$ (see

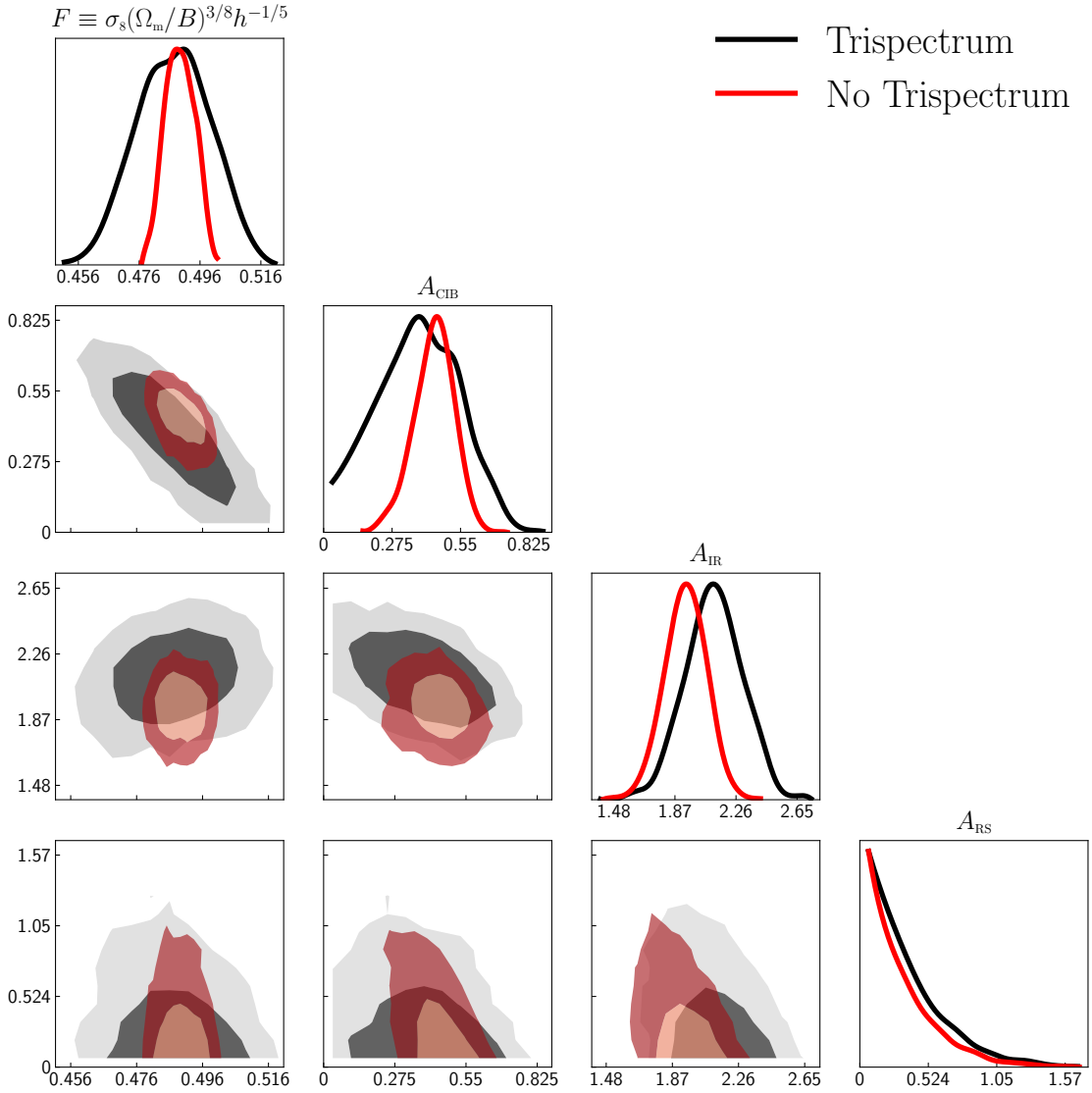

Figure 5: Projected (1D and 2D) joint posterior probability distributions for the F-parameter and the foreground amplitudes from two MCMC analysis, fitting the Planck y^2 power spectrum obtained from the 2015 all-sky y-map. The black contours correspond to the analysis with trispectrum and the red contours to the analysis without trispectrum.

[35] for details), we are able to extract a determination of w which is competitive with CMB TT+lowP+lensing constraints.

We carried out a MCMC analysis assuming a flat wCDM cosmology, where the six base cosmological parameters, the EoS for dark energy, the mass bias, and the three foreground amplitudes were sampled from the uniform priors reported in table I. The resulting contours are shown in black on figure 7. Adding one varying parameter (the EoS) does not alter significantly the constraint on F compared to the ΛCDM case. For the wCDM analysis we get $F = 0.491 \pm 0.016$. As expected, there is no correlation between the F-parameter and the EoS. Hence, measuring F does not allow for a determination of w. Nevertheless, the black contours on figure 7 clearly reveal the underlying correlations between w, σ_8, Ω_m and h.

In a subsequent analysis, we broke these degeneracies by imposing a gaussian prior on h that corresponds to the local measurement of the Hubble parameter [35], as well as the so-called *Normalization prior* on $10^9 A_s e^{-2\tau_{reio}}$ reported in table II. To further reduce the degeneracy, we also set a gaussian prior on the optical depth at reionization $\tau_{reio} = 0.06 \pm 0.01$ that is a good compromise between the different measurements of the last decade [17, 34]. Finally we fixed the value of the mass bias to the one favored by numerical simulations: $B = 1.25$. The resulting contours of this analysis with priors, dubbed tSZ+H_0 on figure 7 are shown in red. The constraint on the F-parameter remains the same as for the analysis without

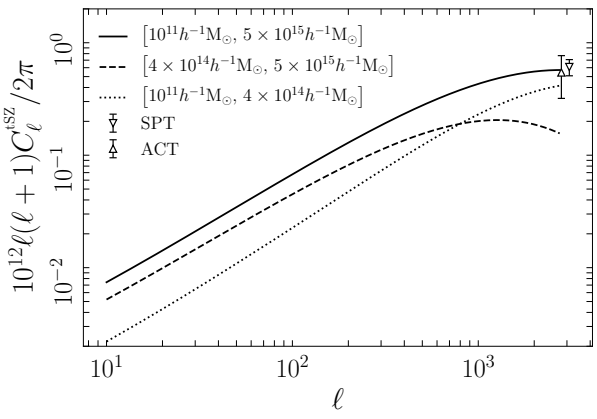

Figure 6: The contributions to the total tSZ power spectrum (solid line) coming from low masses halos (dotted line) and high masses halos (dashed line) computed with `class_sz`. The ACT and SPT data points are shown as a landmark.

priors. Moreover, we get:

$$w = -1.13^{+0.14}_{-0.13}, \tag{28}$$

for the EoS in addition to $\sigma_8 = 0.819 \pm 0.041$, and $\Omega_\mathrm{m} = 0.275 \pm 0.025$. To compare these results with CMB constraints, we use a *compressed* likelihood in order to get the TT+lowP+lensing+H_0 joint posterior probability distribution. The technique of compressed likelihood applied to dark energy related data was initiated in [36]. It is based on the fact that the information contained in the Planck chains for a given model universe (flat, curved, ΛCDM, etc.) can be efficiently recast in the form of a low dimensional covariance matrix for a small set of well chosen cosmological parameter combinations. Then, it is not necessary to re-do the analysis of the Planck observational data, one can use the compressed likelihood instead. Following [37], we constructed the compressed covariance matrix relative to the Planck 2015 TT+lowP+lensing wCDM. The essential parameter combinations that encapsulate the information associated with the background cosmology are the shift parameters, R, and the angular scale of the sound horizon at last scattering ℓ_A. They are given by

$$R \equiv \sqrt{\Omega_\mathrm{m} H_0^2}\, D_\mathrm{A}(z_\star)/c, \tag{29}$$

$$\ell_\mathrm{A} \equiv \pi D_\mathrm{A}(z_\star)/r_* = \pi/\theta_s, \tag{30}$$

where $z_\star$ is the decoupling redshift, $D_\mathrm{A}(z)$ is the comoving angular diameter distance, $r_\star$ is the comoving size of the sound horizon at decoupling and θ_s is the corresponding comoving angular size. In addition, we also use parameters that carry information relative to the dynamics of perturbations, namely: A_s, n_s and $\Omega_b h^2$, leading to a 5x5 covariance matrix. In table IV, we give the *normalized* covariance matrix coefficients, D_{ij}, corresponding to the compressed likelihood. At each step of the MCMC, we compute

$$\chi^2_\mathrm{CMB} = \sum_{i,j=1}^{5} \left(P-\bar{P}\right)_i \left[C^{-1}\right]_{ij} \left(P-\bar{P}\right)_j, \tag{31}$$

where $P \equiv \left\{\Omega_\mathrm{b}h^2, A_\mathrm{s}, n_\mathrm{s}, R, \ell_\mathrm{A}\right\}$ contains the proposed values of the parameters and $\bar{P}$ contains the mean values of the parameters deduced from the wCDM TT+lowP+lensing chains (reported in the first column of the table along with the 68% standard deviations σ_i which enter the covariance matrix coefficients $C_{ij} = \sigma_i\sigma_j D_{ij}$). Then, the χ^2 value for TT+lowP+lensing+H_0 (also denoted CMB+H_0) is given by $\chi^2 = \chi^2_\mathrm{CMB} + \chi^2_{\mathrm{H}_0}$ where $\chi^2_{\mathrm{H}_0}$ corresponds to the priors on h, $10^9 A_s e^{-2\tau_\mathrm{reio}}$ and τ_reio discussed previously (see table II). We find $w_\mathrm{de} = -1.12^{+0.11}_{-0.10}$, $\sigma_8 = 0.844 \pm 0.030$, and $\Omega_\mathrm{m} = 0.275 \pm 0.024$, in good agreement with the tSZ+H_0 analysis and similar width of the 68% C.L. intervals. This shows that the SZ power spectrum is a compelling probe for dark energy, almost as efficient as CMB lensing.

V. SUMMARY AND CONCLUSIONS

In the begining of this article we have reviewed the calculation of the tSZ power spectrum and trispectrum based on the halo model. We have implemented it in a new module for `CLASS` and made it publicly available on the internet.

We reconciled `szfast` based analysis and the Planck analysis by identifying the source of the discrepancy: it is due to the use of the concentration mass relation for the conversion from the halo masses to the over-density mass.

Then, we revisited the Planck 2015 analysis of the tSZ power spectrum and updated the tSZ data with the inclusion of the trispectrum in the covariance matrix, as well as varying the whole set of cosmological parameters instead of only σ_8 and Ω_m. We found a larger foreground contribution and a smaller tSZ component to the total y^2 power spectrum than PLC15. Our updated tSZ data is now in perfect agreement with the ACT/SPT measurements at higher multipoles.

We saw that the parameter that is determined by the SZ data is the F-parameter, which accounts for the fact that the amplitude of the tSZ power spectrum is not only set by σ_8 and Ω_m but also by the the Hubble parameter and the mass bias.

We used CMB constraints on σ_8, Ω_m and h to obtain an estimate of the mass bias, which was found to be in good agreement with weak lensing estimates and in perfect agreement with the SZ number counts constraint and the prediction for large masses halos from numerical simulations.

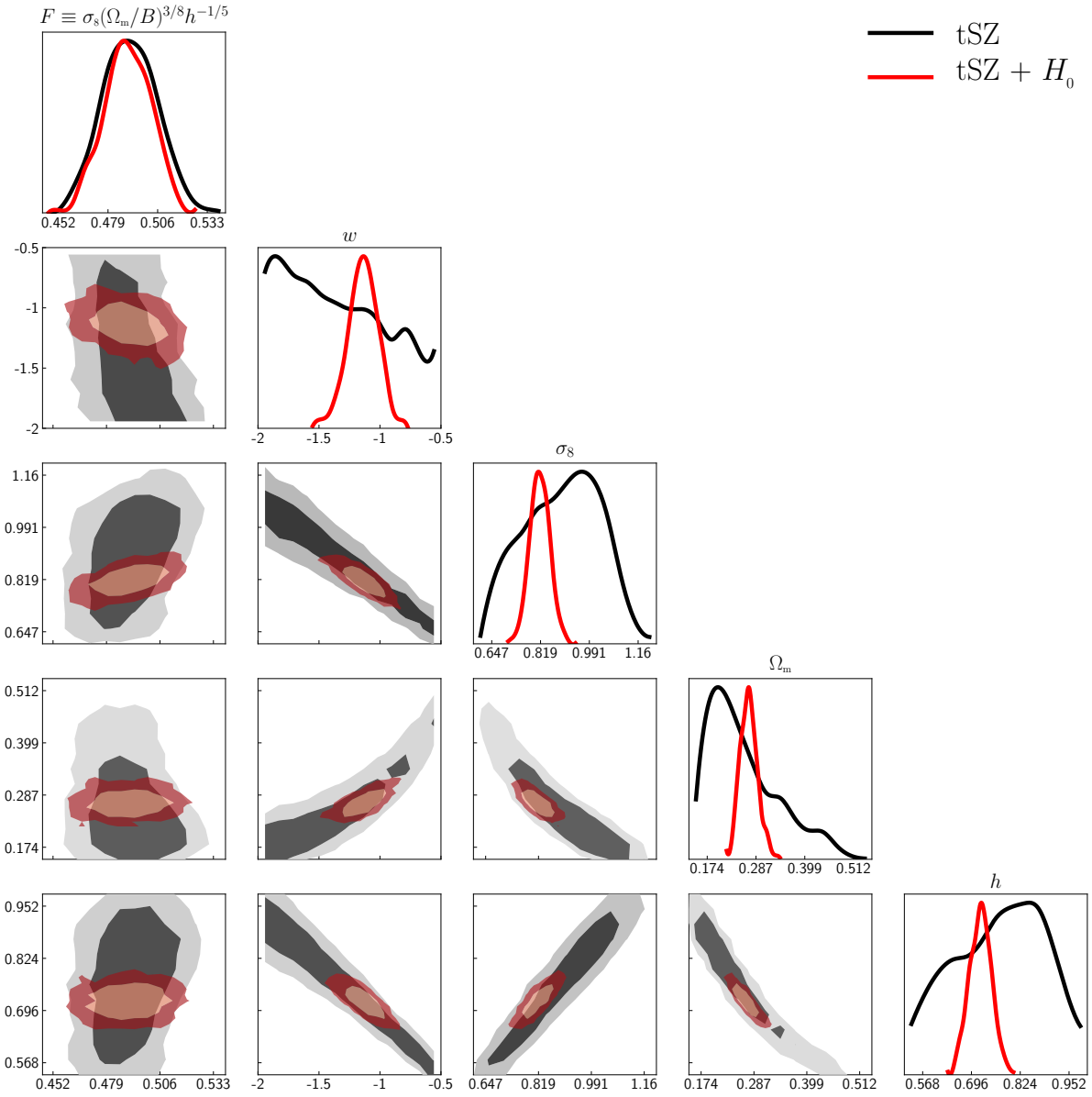

Figure 7: Projected (1D and 2D) joint posterior probability distribution as obtained from the "tSZ" analysis (all parameters varying including the mass bias B and the equation of state of dark energy w) and the "tSZ + H_0" analysis for which we set the bias to $B = 1.25$ and imposed priors on h, $A_s e^{-2\tau_{\rm reio}}$ and $\tau_{\rm reio}$ (see table II).

Finally, we used the lattest local measurement of the Hubble parameter and the Planck 2015 normalization prior in order to constrain the equation of state of dark energy from the SZ data. We shown that the tSZ power spectrum is actually a powerful probe of dark energy, competitive with CMB weak lensing.

Acknowledgment

BB is very grateful to Guillaume Hurier, Scott Kay, Fabien Lacasa, Ryu Makiya and Florian Ruppin.

Appendix : SZ Data, Compressed Likelihood and Normalization Priors

	Gaussian priors
h	0.72 ± 0.03
$10^9 A_s e^{-2\tau_{\rm reio}}$	1.878 ± 0.014
$\tau_{\rm reio}$	0.06 ± 0.01

Table II: Gaussian priors imposed on the parameters h, $10^9 A_s e^{-2\tau_{\rm reio}}$ and $\tau_{\rm reio}$ (in order to break the degeneracy between $w_{\rm de}$ and other cosmological parameters in the tSZ wCDM analysis). The prior on h is from [35] (quasars time delay), the prior on $A_s e^{-2\tau_{\rm reio}}$ was obtained from the Planck chains (see table III) and the prior on the optical depth is a compromise between the different measurements over the last decade.

	$10^9 A_s e^{-2\tau_{\rm reio}}$
$\Omega_{\rm k}=0$ and $w=-1$	1.880 ± 0.014
$\Omega_{\rm k}\neq 0$ and $w=-1$	1.872 ± 0.014
$\Omega_{\rm k}=0$ and $w\neq -1$	1.880 ± 0.014
$\Omega_{\rm k}=0$ and $w=-1$ and $m_\nu>0$	1.881 ± 0.014
Normalization prior	1.878 ± 0.014

Table III: The constraints on $10^9 A_s e^{-2\tau_{\rm reio}}$, with pivot scale $k = 0.05{\rm Mpc}^{-1}$, are read out of four sets of Planck 2015 chains (corresponding to the first four lines of the table) in order to deduce the Planck 2015 model independent *normalization* prior on this parameter combination.

	68% C.L.	$\Omega_{\rm b}h^2$	$10^9 A_{\rm s}$	$n_{\rm s}$	R	$\ell_{\rm A}$
$\Omega_{\rm b}h^2$	0.02228 ± 0.00024	1	0.39	0.61	−0.66	−0.44
$10^9 A_{\rm s}$	2.1108 ± 0.0713	0.39	1	0.60	−0.58	−0.37
$n_{\rm s}$	0.9681 ± 0.0057	0.61	0.60	1	−0.85	−0.45
R	1.7447 ± 0.0068	−0.66	−0.58	−0.85	1	0.51
$\ell_{\rm A}$	301.70 ± 0.14	−0.44	−0.37	−0.45	0.51	1

Table IV: Normalized compressed likelihood for the Planck 2015 TT+lowP+lensing (wCDM) chains. The first column gives the the mean values and 68%CL standard deviations. The last five columns are the coefficients D_{ij} of the normalized covariance matrix. The shift parameter R is defined in Eq. (30).

[1] R. A. Sunyaev and Y. B. Zeldovich, Comments on Astrophysics and Space Physics **4**, 173 (1972).

[2] P. A. R. Ade et al. (Planck), Astron. Astrophys. **594**, A24 (2016), 1502.01597.

[3] N. Kaiser, mnras **222**, 323 (1986).

[4] A. C. da Silva, S. T. Kay, A. R. Liddle, and P. A. Thomas, Mon. Not. Roy. Astron. Soc. **348**, 1401 (2004), astro-ph/0308074.

[5] X. Shi and E. Komatsu, Mon. Not. Roy. Astron. Soc. **442**, 521 (2014), 1401.7657.

[6] G. Hurier, J. Macias-Perez, and S. Hildebrandt, Astronomy and Astrophysics - A&A **558**, A118 (2013), 8 pages, URL http://hal.in2p3.fr/in2p3-00498624.

[7] M. Remazeilles, J. Delabrouille, and J.-F. Cardoso, mnras **410**, 2481 (2011), 1006.5599.

[8] N. Aghanim et al. (Planck), Astron. Astrophys. **594**, A22 (2016), 1502.01596.

[9] G. Hurier and F. Lacasa, Astron. Astrophys. **604**, A71 (2017), 1701.09067.

[10] M. Tristram, J. F. Macias-Perez, C. Renault, and D. Santos, Mon. Not. Roy. Astron. Soc. **358**, 833 (2005), astro-ph/0405575.

[11] Planck Collaboration, P. A. R. Ade, N. Aghanim, M. Arnaud, M. Ashdown, J. Aumont, C. Baccigalupi, A. J. Banday, R. B. Barreiro, J. G. Bartlett, et al., aap **594**, A12 (2016), 1509.06348.

[12] P. A. R. Ade et al. (Planck), Astron. Astrophys. **594**, A23 (2016), 1509.06555.

[13] E. Komatsu and U. Seljak, Mon. Not. Roy. Astron. Soc. **336**, 1256 (2002), astro-ph/0205468.

[14] B. Horowitz and U. Seljak (2016), 1609.01850.

[15] K. Dolag, E. Komatsu, and R. Sunyaev, Mon. Not. Roy. Astron. Soc. **463**, 1797 (2016), 1509.05134.

[16] L. Salvati, M. Douspis, and N. Aghanim (2017), 1708.00697.

[17] E. Komatsu, K. M. Smith, J. Dunkley, C. L. Bennett, B. Gold, G. Hinshaw, N. Jarosik, D. Larson, M. R. Nolta, L. Page, et al., Astrophys. J. Suppl. **192**, 18 (2011), 1001.4538.

[18] Planck Collaboration, P. A. R. Ade, N. Aghanim, M. Arnaud, M. Ashdown, F. Atrio-Barandela, J. Aumont, C. Baccigalupi, A. Balbi, A. J. Banday, et al., Astron. Astrophys. **550**, A131 (2013), 1207.4061.

[19] M. Arnaud, G. W. Pratt, R. Piffaretti, H. Böhringer, J. H. Croston, and E. Pointecouteau, aap **517**, A92 (2010), 0910.1234.

[20] J. L. Tinker, B. E. Robertson, A. V. Kravtsov, A. Klypin, M. S. Warren, G. Yepes, and S. Gottlöber, Astrophys. J. **724**, 878 (2010), 1001.3162.

[21] S. Bocquet, A. Saro, K. Dolag, and J. J. Mohr, Mon. Not. Roy. Astron. Soc. **456**, 2361 (2016), 1502.07357.

[22] J. L. Tinker, A. V. Kravtsov, A. Klypin, K. Abazajian, M. S. Warren, G. Yepes, S. Gottlober, and D. E. Holz, Astrophys. J. **688**, 709 (2008), 0803.2706.

[23] A. Jenkins, C. S. Frenk, S. D. M. White, J. M. Colberg, S. Cole, A. E. Evrard, H. M. P. Couchman, and N. Yoshida, Mon. Not. Roy. Astron. Soc. **321**, 372 (2001), astro-ph/0005260.

[24] A. R. Duffy, J. Schaye, S. T. Kay, and C. Dalla Vecchia, Mon. Not. Roy. Astron. Soc. **390**, L64 (2008), [Erratum: Mon. Not. Roy. Astron. Soc.415,L85(2011)], 0804.2486.

[25] A. A. Klypin, S. Trujillo-Gomez, and J. Primack, apj **740**, 102 (2011), 1002.3660.

[26] M. A. Sánchez-Conde and F. Prada, Mon. Not. Roy. Astron. Soc. **442**, 2271 (2014), 1312.1729.

[27] D. H. Zhao, Y. P. Jing, H. J. Mo, and G. Boerner, Astrophys. J. **707**, 354 (2009), 0811.0828.

[28] P. A. R. Ade et al. (Planck), Astron. Astrophys. **571**, A21 (2014), 1303.5081.

[29] B. Audren, J. Lesgourgues, K. Benabed, and S. Prunet, JCAP **2**, 001 (2013), 1210.7183.

[30] A. Lewis, Phys. Rev. **D87**, 103529 (2013), 1304.4473.

[31] M. Simet, N. Battaglia, R. Mandelbaum, and U. Seljak, Mon. Not. Roy. Astron. Soc. **466**, 3663 (2017), 1502.01024.

[32] M. Penna-Lima, J. G. Bartlett, E. Rozo, J. B. Melin, J. Merten, A. E. Evrard, M. Postman, and E. Rykoff, Astron. Astrophys. **604**, A89 (2017), 1608.05356.

[33] M. A. Henson, D. J. Barnes, S. T. Kay, I. G. McCarthy, and J. Schaye, Mon. Not. Roy. Astron. Soc. **465**, 3361 (2017), 1607.08550.

[34] P. A. R. Ade et al. (Planck), Astron. Astrophys. **594**, A13 (2016), 1502.01589.

[35] J. L. Bernal, L. Verde, and A. G. Riess, JCAP **1610**, 019 (2016), 1607.05617.

[36] P. Mukherjee, M. Kunz, D. Parkinson, and Y. Wang,

$\ell_{\rm eff}$	$C_\ell^{y^2}$	$\sigma_\ell^{y^2}$	$C_\ell^{\rm RC}$	$\sigma_\ell^{\rm RC}$	$C_\ell^{\rm CIB}$	$C_\ell^{\rm RS}$	$C_\ell^{\rm IR}$	$C_\ell^{\rm CN}$
10	0.00508	0.00629	0.000421	0.000160	0.000000	0.000043	0.000007	0.000001
13.5	0.00881	0.00615	0.000710	0.000192	0.000000	0.000142	0.000024	0.000001
18	0.01363	0.00579	0.001251	0.000254	0.000000	0.000296	0.000048	0.000002
23.5	0.02961	0.00805	0.002837	0.000446	0.000000	0.000400	0.000073	0.000004
30.5	0.02241	0.00521	0.003933	0.000460	0.000902	0.000541	0.000111	0.000006
40	0.02849	0.00464	0.005969	0.000510	0.002010	0.001056	0.000224	0.000010
52.5	0.04276	0.00468	0.010318	0.000672	0.003119	0.001647	0.000449	0.000018
68.5	0.04580	0.00429	0.014045	0.000699	0.006278	0.002787	0.000837	0.000030
89.5	0.07104	0.00454	0.024061	0.000896	0.012242	0.004306	0.001400	0.000052
117	0.11914	0.00562	0.032976	0.000936	0.021584	0.006842	0.002701	0.000089
152.5	0.15150	0.00594	0.04710	0.00102	0.045915	0.011264	0.004721	0.000153
198	0.19390	0.00611	0.06238	0.00104	0.070582	0.016744	0.008115	0.000262
257.5	0.28175	0.00687	0.08173	0.00103	0.119786	0.027345	0.014618	0.000456
335.5	0.39837	0.00824	0.101911	0.000978	0.211686	0.043275	0.024893	0.000815
436.5	0.56743	0.00958	0.117412	0.000860	0.332863	0.070587	0.051570	0.001503
567.5	0.76866	0.01242	0.132234	0.000769	0.434931	0.115356	0.107293	0.002934
738	1.1101	0.0165	0.143214	0.000642	0.602030	0.154926	0.197053	0.006334
959.5	1.6614	0.0240	0.156202	0.000544	0.754733	0.207200	0.361713	0.016171
1247.5	2.5217	0.0417	0.175341	0.000492	1.029014	0.287652	0.681036	0.054883
1622	4.5851	0.0987	0.283969	0.000900	1.357567	0.410274	1.295272	0.301480
2109	12.269	0.401	1.36368	0.00365	1.850146	0.657659	2.534448	3.738250
2742	165.6	23.6	54.69	2.31	2.629002	1.117189	4.545315	183.267263

Table V: Planck 2015 data points and error bars for the y^2 power spectrum from the all-sky y-map, $C_\ell^{y^2}$, the SZ resolved cluster catalogue $C_\ell^{y^2}$, and models for the foreground contributions: cosmic infrared background (CIB), infrared sources (IR) and radio sources (RS). Data points were taken from [8]. The last column is the correlated noise of the instrument, see [10]. The numerical values correspond to the rescaled dimensionless power spectra $10^{12}\ell\,(\ell+1)\,C_\ell/2\pi$ and error bars. Only the first eighteen multipole bins (up to $\ell = 959.5$) are fitted in our MCMC analysis. The last data point at $\ell_{\rm eff} = 2742$ is used for the determination of the correlated noise amplitude.

Phys. Rev. **D78**, 083529 (2008), 0803.1616.

[37] Y. Wang and M. Dai, Phys. Rev. **D94**, 083521 (2016), 1509.02198.